The Use of Nonnatural Nucleotides to Probe the Contributions of Shape Complementarity and π-Electron Surface Area during DNA Polymerization†

Xuemei Zhang,‡ Irene Lee,§ and Anthony J. Berdis*,‡

Departments of Pharmacology and Chemistry, Case Western Reserve University, 10900 Euclid Avenue, Cleveland, Ohio 44106

Received March 30, 2005; Revised Manuscript Received June 27, 2005

ABSTRACT: It is widely accepted that the dynamic behavior of DNA polymerases during translesion DNA synthesis is dependent upon the nature of the DNA lesion and the incoming dNTP destined to be the complementary partner. We previously demonstrated that 5-nitro-1-indolyl-2′-deoxyribose-5′-triphosphate, a nonnatural nucleobase possessing enhanced base-stacking abilities, can be selectively incorporated opposite an abasic site (Reineks, E. Z., and Berdis, A. J. (2004) *Biochemistry 43*, 393−404.). While the enhancement in insertion presumably reflected the contributions of the π-electrons present in the nitro group, other physical parameters such as solvation capabilities, dipole moment, surface area, and shape could also contribute. To evaluate these possibilities, a series of 5-substituted indole triphosphates were synthesized and tested for enzymatic incorporation into normal and damaged DNA by the bacteriophage T4 DNA polymerase. The overall catalytic efficiency for the insertion of the 5-phenyl-indole derivative opposite an abasic site is several orders of magnitude greater than the insertion of either the 5-fluoro- or the 5-amino-indole derivative. The generated structure−activity relationship indicates that π-electrons play the largest role in modulating the catalytic efficiency for insertion opposite this nontemplating DNA lesion. Despite the large size of 5-phenyl-indole, the catalytic efficiency for its insertion opposite natural nucleobases is equal to or greater than that of the 5-fluoro- or 5-amino-indole derivatives. The higher catalytic efficiency reflects a higher binding affinity of 5-phenyl-1-indolyl-2′-deoxyribose-5′-triphosphate and suggests that the polymerase relies on π-electron surface area rather than shape complementarity as a driving force for polymerization efficiency.

Hydrogen-bonding, base-stacking, and solvation/desolvation contributions play significant roles in maintaining the stability of nucleic acid (reviewed in ref *1*). Perhaps the most elusive question in nucleic acid metabolism is the extent to which each of these molecular forces is efficiently utilized by DNA polymerases during replication. The individual contributions of these forces during the polymerization process have been difficult to dissect due to the paradoxical nature of the nucleobases that compose DNA. Specifically, in addition to base-stacking capabilities, each nucleobase contains functional groups capable of hydrogen-bond interactions with water as well as with other acceptor−donor groups on other nucleobases.

Several laboratories have attempted to deconvolute this paradox by monitoring the kinetics of insertion of nonnatural nucleosides devoid of classical hydrogen bonding groups (*2*−*6*). The collective results of these studies indicate that the presence of hydrogen-bonding groups is not an absolute requirement for the stable incorporation of a nonnatural nucleobase into DNA (*2*−*6*). In most instances, a nonnatural nucleoside is preferentially inserted opposite the complementarity partner of its isosteric progenitor. This kinetic phenomenon was originally interpreted to reflect the contributions of geometrical constraints of the formed base pair (*6*). However, other molecular forces such as base stacking and desolvation cannot be eliminated since they also play significant roles during DNA polymerization.

To evaluate the contributions of these parameters, we have examined the dynamics of nucleoside insertion opposite an abasic site, a nontemplating DNA lesion devoid of classical hydrogen-bonding potential as well as normal size/shape constraints. Many DNA polymerases such as the eukaryotic polymerases pol α (*7*) and pol δ (*8*), the Klenow fragment from *E. coli* (*9*, *10*), HIV reverse transcriptase, (*11*, *12*), and gp43 from bacteriophage T4 (*13*) preferentially insert dAMP (and dGMP to a lesser extent) opposite an abasic site. An attractive mechanism to explain this kinetic phenomenon is that polymerization efficiency is influenced more by the base-stacking capabilities of the incoming dNTP[1] rather than its size or shape (*13*). The validity of this hypothesis has been strengthened by the favorable enzymatic insertion of 5-NIMP opposite an abasic site (*14*). Although 5-NITP does not possess "classical" hydrogen-bonding acceptor/donor groups,

† This research was supported through funding from the American Cancer Society Cuyahoga Unit to A.J.B. (Grant 021203A) and from the Presidential Research Initiative to I.L.

* Corresponding author: Telephone (216)-368-4723, fax (216) 368-3395, e-mail ajb15@cwru.edu.

‡ Department of Pharmacology.

§ Department of Chemistry.

[1] Abbreviations: TBE, Tris-HCl/borate/EDTA; EDTA; ethylenediaminetetraacetate, sodium salt; dNTP, deoxynucleoside triphosphate; dXTP, nonnatural deoxynucleoside triphosphate; 5-NITP, 5-nitro-indolyl-2′-deoxyriboside triphosphate; Ind-TP, indolyl-2′-deoxyriboside triphosphate; 5-PhITP, 5-phenyl-indolyl-2′-deoxyriboside triphosphate; 5-FITP, 5-fluoro-indolyl-2′-deoxyriboside triphosphate; 5-AITP, 5-amino-indolyl-2′-deoxyriboside triphosphate; gp43 exo$^-$, an exonuclease-deficient mutant of the bacteriophage T4 DNA polymerase.

10.1021/bi050585f CCC: $30.25
Published on Web 09/03/2005

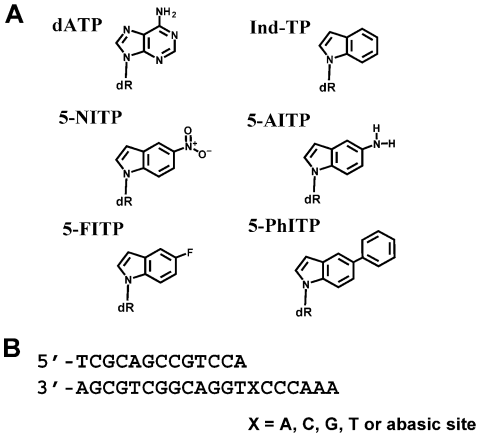

FIGURE 1: (A) Structures of 2′-deoxynucleoside triphosphates used or referred to in this study, dATP, 5-NITP, Ind-TP, 5-PhITP, 5-FITP, and 5-AITP. For convenience, dR is used to represent the deoxyribose triphosphate portion of the nucleotides. (B) Defined DNA substrates used for kinetic analysis. "X" in the template strand denotes any of the four natural nucleobases or the presence of a tetrahydrofuran moiety designed to mimic an abasic site.

it has enhanced base-stacking capabilities compared to natural dNTPs (*15*). Remarkably, the catalytic efficiency for 5-NIMP insertion opposite the lesion is 1000-fold greater than that measured for the insertion of dAMP (*14*). The nitro moiety appears to play an important role since replacement with −H reduces the catalytic efficiency for nucleoside insertion by ∼2300-fold (*16*). Although binding affinity is perturbed slightly, the major effect of this substitution is the 450-fold reduction in the rate of the conformational change step that corresponds to a change in relative free energy ($\Delta\Delta G$) of 3.62 kcal/mol (*16*). This energetic difference was proposed to arise through base-stacking interactions mediated between the overlapping π-electron densities of the conjugated indole nucleoside with the polymerase and DNA (*14*, *16*). However, other forces such as desolvation as well as size and shape complementarity cannot be unambiguously refuted based solely upon these data.

In this report, we have further evaluated the contribution of base stacking, desolvation, shape, and dipole moment toward translesion DNA synthesis by measuring the insertion of various 5-substituted indolyl-2′-deoxyribose triphosphates displayed in Figure 1A. Of the analogues examined, 5-phenyl-indolyl-2′-deoxyribose triphosphate displays the highest catalytic efficiency for insertion opposite the abasic site. The generated structure−activity relationships provide evidence that π-electron surface area rather than size, shape, or desolvation capabilities is the most important factor for insertion opposite an abasic lesion. When tested for insertion opposite templating nucleobases, the expected correlation between insertion efficiency and shape complementarity of the formed base pair is not observed. Collectively, these results suggest that steric fit plays a minimal role during polymerization catalyzed by the bacteriophage T4 DNA polymerase.

METHODS AND MATERIALS

Materials. [γ-^{32}P]ATP was purchased from M. P. Biomedical (Irvine, CA). Unlabeled dNTPs (ultrapure) were obtained from Pharmacia. Magnesium acetate and Trizma base were from Sigma. Urea, acrylamide, and bisacrylamide were from Aldrich. Oligonucleotides, including those containing a tetrahydrofuran moiety mimicking an abasic site, were synthesized by Operon Technologies (Alameda, CA). Single-stranded and duplex DNA were purified and quantified as described (*17*). All other materials were obtained from commercial sources and were of the highest available quality. The exonuclease-deficient mutant of gp43 (Asp-219 to Ala mutation) was purified and quantified as previously described (*18*, *19*).

Tributylammonium pyrophosphate was purchased from Sigma. 5-Fluoro-indole, 1-chloro-2-deoxy-3,5-di-*O*-*p*-toluoyl-α-D-*erythro*-pentofuranose, ethyl acetate, hexane, methanol, dichloromethane, phosphoryl oxychloride, dimethyl formamide, and tributylamine were purchased from ACROS. Trimethyl phosphate and tributylamine were dried over 4 Å molecular sieves. DMF was distilled from ninhydrin and stored in 4 Å molecular sieves.

All NMR spectra were record in a Gemini-300 FT NMR spectrometer. Proton chemical shifts are reported in ppm downfield from tetramethylsilane. Coupling constants (*J*) are reported in hertz (Hz). ^{31}P NMR spectra were taken in D_2O in the presence of 50 mM Tris (pH 7.5) and 2 mM EDTA. Phosphoric acid (85%) was used as external standard. Ultraviolet quantification of triphosphate was performed on Beckman DU-70. High-resolution electrospray mass spectrometry (negative) was performed on Ionspec HiRES ESI-FTICRMS at the University of Cincinnati.

Synthesis of 5-Fluoro-indole-2′-deoxyribofuranoside 5′-Triphosphate (5-FITP). The 5-fluoro-indole deoxyriboside was synthesized similarly to a previous report (*16*, *20*). The 5-fluoro-indole-2′-deoxynucleoside was converted to the triphosphate form first by reaction with phosphoryl oxychloride in the presence of proton sponge and trimethyl phosphate. After 2 h, the reaction was simultaneously treated with a 0.5 M solution of tributylammonium pyrophosphate and tributylamine in dimethyl formamide. The desired compound was purified by semipreparative reverse-phase HPLC (300 pore size C-18 column from Vydac, 10 mm × 250 mm) with mobile phase buffer A = 0.1 M TEAB and buffer B = 35% ACN in 0.1 M TEAB, using a linear gradient from 45% to 80% B within 18 min at a flow rate of 2.3 mL/min. The desired triphosphate was eluted at 73% B (14 min retention time). After concentration and evaporation, the final product was dissolved and stored in 10 mM TrisHCl, pH 7.5, and 1 mM EDTA. The concentration was determined using an extinction coefficient of 6142 M^{-1} cm^{-1} for the free nucleoside. The yield of phosphorylation was 20%. 1-(3,5-Di-*O*-*p*-toluoyl-2-deoxy-β-D-*erythro*-pentafuranosyl)-5-fluoro-indole (**1a**): H NMR (DMSO) 2.37 (3H, s, CH_3), 2.40 (3H, s, CH_3), 2.69 (1H, m, 2′-H), 2.96 (1H, m, 2′-H), 4.45−4.65 (3H, m, 5′-H, 4′-H), 5.60−5.70 (1H, m, 3′-H), 6.51 (1H, d, J = 3.3 Hz, 3-H), 6.59 (1H, t, J = 6.0 Hz, 1′-H), 6.87−6.94 (1H, m, Ar), 7.30−7.38 (5H, m, Ar), 7.66−7.70 (2H, m, Ar), 7.88 (2H, d, J = 8 Hz, Ar), 7.99 (2H, d, J = 8 Hz, Ar). 1-(2-Deoxy-β-D-*erythro*-pentafuranosyl)-5-fluoro-indole: H NMR (DMSO) 2.25 (1H, m, 2′-H), 2.55 (1H, m, 2′-H), 3.45−3.55 (2H, m, 5′-H), 3.83−3.88 (1H, m, 4′-H), 4.32−4.34 (1H, m, 3′-H), 4.90 (1H, m, 5′-OH), 5.30 (1H, m, 3′-OH), 6.34 (1H, t, J = 6.9 Hz, 1′-H), 6.45 (1H, d, J = 3.4 Hz, 3-H), 6.90 (1H, m, Ar), 7.32 (1 H, m, Ar), 7.57−7.66 (2H, m, Ar). 1-(2-Deoxy-β-D-*erythro*-pentafuranosyl)-5-fluoro-indole triphosphate (5-FITP): ^{31}P

NMR (ppm) (D_2O/Tris/EDTA) γ-P −5.75 (d); α-P −10.22 (d); β-P −21.50 (t). HiRes ESI-MS (−): Calculated mass spec (formula $C_{13}H_{16}FNO_{12}P_3$ for M − H) = 489.9869. Experimental mass spec = 490.0164.

Synthesis of 5-Phenyl-indole-2′-Deoxyribofuranoside 5′-Triphosphate (5-PhITP). 5-Phenyl-indole was synthesized using established protocols (*21*, *22*). 1-(2-Deoxy-β-D-*erythro*-pentafuranosyl)-5-phenyl-indole was prepared by the method described for deprotection of fluoro-indole nucleoside. The overall yield of the reaction was 70%. 1-(2-Deoxy-β-D-*erythro*-pentafuranosyl)-5-phenyl-indole triphosphate (PhITP) was prepared starting with 5-phenyl-indole-2′-deoxynucleoside. The residue was purified by preparative reverse phase HPLC (300 pore size C-18 column from Vydac, 22 mm × 250 mm) with mobile phase buffer A = 0.1 M TEAB and buffer B = 35% ACN in 0.1 M TEAB. The reaction mixture was purified using 80% B without gradient. The product was eluted at 24 min retention time with a flow rate of 4.5 mL/min. The final product was dissolved and stored in 10 mM TrisHCl, pH 7.5. The concentration of nucleotide was determined using the extinction coefficient of 35 379 M^{-1} cm^{-1} determined for the free nucleoside. 1-(3,5-Di-*O*-*p*-toluoyl-2-deoxy-β-D-*erythro*-pentafuranosyl)-5-phenyl-indole (**1b**): H NMR ($CDCl_3$) 2.41, (3H, s, CH_3), 2.45 (3H, s, CH_3), 2.70 (1H, m, 2′-H), 2.78 (1H, m, 2′-H), 4.5−4.65 (3H, m, 5′-H, 4′-H), 5.72 (1H, m, 3′-H), 6.58 (1H, d, J = 3.3 Hz, 3-H), 6.62 (1H, t, J = 7.2 Hz, 1′-H), 7.31−7.50 (8H, m, Ar), 7.60−8.06 (9H, m, Ar). 1-(2-Deoxy-β-D-*erythro*-pentafuranosyl)-5-phenyl-indole: H NMR (DMSO) 2.25 (1H, m, 2′-H), 2.55 (1H, m, 2′-H), 3.52−3.62 (2H, m, 5′-H), 3.83−3.88 (1H, m, 4′-H), 4.34−4.41 (1H, m, 3′-H), 4.90 (1H, t, J = 5 Hz, 5′-OH), 5.30 (1H, d, J = 4 Hz, 3′-OH), 6.40 (1H, t, J = 6.2 Hz, 1′-H), 6.56 (1H, d, J = 3.3 Hz, 3-H), 7.30−7.33 (1H, m, Ar), 7.41−7.45 (3H, m, Ar), 7.61−7.67 (4H, m, Ar), 7.81 (1H, d, J = 2 Hz, Ar). 1-(2-Deoxy-β-D-*erythro*-pentafuranosyl)-5-phenyl-indole triphosphate (PhITP) ^{31}P NMR (ppm) (D_2O/Tris/EDTA) γ-P −5.65 (d); α-P −10.35 (d); β-P −21.46 (t). HiRes ESI-MS (−): Calculated mass spec (formula $C_{19}H_{21}N_1O_{12}P_3$ for M − H) = 548.0277. Experimental mass spec = 548.0242.

Synthesis of 5-Amino-Indole-2′-Deoxyribofuranoside 5′-Triphosphate (5-AITP). Amino-indole triphosphate was prepared from 5-nitro-indole triphosphate by hydrogenation reaction as described (*23*). The extinction coefficient for 5-amino-indole is 5830 $M^{-1}cm^{-1}$ at 270 nm.

Enzyme Assays. The assay buffer used in all kinetic studies consisted of 25 mM Tris-OAc (pH 7.5), 150 mM KOAc, and 10 mM 2-mercaptoethanol. All assays were performed at 25 °C. Polymerization reactions were monitored by analysis of the products on 20% sequencing gels as previously described (*24*). Gel images were obtained with a Packard PhosphorImager using the OptiQuant software supplied by the manufacturer. Product formation was quantified by measuring the ratio of ^{32}P-labeled extended and nonextended primer. The ratios of product formation are corrected for substrate in the absence of polymerase (zero point). Corrected ratios are then multiplied by the concentration of primer/template used in each assay to yield total product. All concentrations are listed as final solution concentrations.

The kinetic parameters, k_{cat}, K_m, and k_{cat}/K_m, for each nonnatural nucleotide were obtained by monitoring the rate of product formation using a fixed amount of gp43 (50 nM) and DNA substrate (1000 nM) at varying concentrations of nucleotide triphosphate (0.01−1 mM). Aliquots of the reaction were quenched into 0.5 M EDTA, pH 7.4, at times ranging from 5 to 600 s. Samples were diluted 1:1 with sequencing gel loading buffer and products were analyzed for product formation by denaturing gel electrophoresis. In all cases, steady-state rates were obtained from the linear portion of the time course. Data obtained for steady-state rates in DNA polymerization measured under pseudo-first-order reaction conditions were fit to eq 1:

$$y = mt + b \tag{1}$$

where m is the slope of the line, b is the y-intercept, and t is time. The slope of the line is equivalent to the rate of the reaction, ν, and has units of nM/s. Data for the dependency of ν as a function of dXTP concentration were fit to the Michaelis−Menten equation:

$$\nu = V_{max}[\text{dXTP}]/K_m + [\text{dXTP}] \tag{2}$$

where ν is the rate of the reaction, V_{max} is the maximal velocity, K_m is the Michaelis constant for dXTP, and [dXTP] is the concentration of nonnatural nucleotide substrate. k_{cat} is defined as V_{max}/[gp43].

Pre-Steady-State Nucleotide Incorporation Assays. A rapid quench instrument (KinTek Corporation, Clarence, PA) was used to monitor the time course in 5-PhIMP insertion using 13/20SP-mer or 13/20T-mer as the DNA substrate. A preincubated solution of 75 nM gp43 exo$^-$ polymerase and 2000 nM 5′-labeled DNA (final concentrations) was mixed with an equal volume of a solution containing 10 mM magnesium acetate and 10 μM 5-PhITP (final concentrations) in the same reaction buffer. The reaction was then terminated at various times by the addition of 350 mM EDTA. Polymerization products were analyzed as described above. Data for each time course were fit to eq 3 defining a burst in product formation followed by a steady-state rate.

$$y = A\,e^{-kt} + Bt + C \tag{3}$$

where A is the burst amplitude, k is the observed rate constant for initial product formation, B is the steady-state rate, t is time, and C is a defined constant.

In some instances, experiments were performed using single turnover reaction conditions. One thousand nanomolar gp43 exo$^-$ was incubated with 250 nM DNA in assay buffer containing EDTA (100 μM) and mixed with variable concentrations of nucleotide analogue (5−500 μM) and 10 mM magnesium acetate. The reactions were quenched with 500 mM EDTA at variable times (0.005−10 s) and analyzed as described above. Data obtained for single turnover DNA polymerization assays were fit to eq 4.

$$y = A\,e^{-kt} + C \tag{4}$$

where A is the burst amplitude, k is the observed rate constant for initial product formation, t is time, and C is a defined constant. Data for the dependency of k_{obs} as a function of dNTP concentration was fit to the Michaelis−Menten equation (eq 2) to provide values corresponding to k_{pol} and K_D.

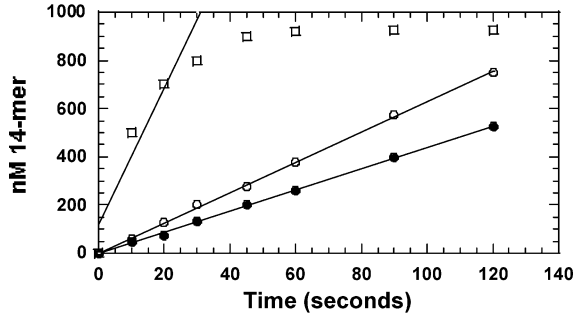

FIGURE 2: Time courses in the incorporation of 250 μM 5-AITP (●), 150 μM 5-FITP (○), and 15 μM 5-PhITP (□) opposite an abasic site. All reactions were performed using pseudo-first-order reaction conditions (50 nM gp43 exo$^-$/1000 nM 13/20SP-mer). Extrapolation of the time course back to time zero does not reveal a burst in product formation using 5-AITP or 5-FITP. In contrast, an apparent burst in primer elongation is observed using a significantly lower concentration of 5-PhITP.

Table 1: Summary of Kinetic Rate and Equilibrium Constants Measured for the Insertion of 5-Substituted Indolyl-2′-deoxyriboside Triphosphates Opposite an Abasic Site

analogue	k_{pol} (s^{-1})	K_D (μM)	k_{pol}/K_D (M^{-1} s^{-1})
5-PhITP[a]	53 ± 4	14 ± 3	3.8×10^6
5-FITP[b]	0.30 ± 0.03	152 ± 41	2.0×10^3
5-AITP[b]	0.17 ± 0.01	255 ± 43	0.7×10^3
5-NITP[c]	126 ± 6	18 ± 3	7.0×10^6
IndTP[d]	0.28 ± 0.07	145 ± 10	1.9×10^3

[a] The kinetic parameters, k_{pol}, K_D, and k_{pol}/K_D, were obtained under single turnover conditions using 1 μM gp43exo$^-$, 250 nM 13/20SP-mer, and 10 mM Mg^{2+} at varying concentrations of nonnatural nucleotide triphosphate (0.0025−0.100 mM). [b] The kinetic parameters were obtained under pseudo-first-order reaction conditions using 50 nM gp43exo$^-$, 1 μM 13/20SP-mer, and 10 mM Mg^{2+} at varying concentrations of nonnatural nucleotide triphosphate (0.01−1 mM). [c] Values taken from Reineks and Berdis (*14*). [d] Values taken from Zhang et al. (*16*).

RESULTS

Steady-State Kinetic Parameters for Insertion Opposite an Abasic Site. The kinetic parameters, k_{pol}, K_D, and k_{pol}/K_D for each substituted indole triphosphate during incorporation opposite an abasic site were obtained by monitoring the rate of product formation at varying nucleotide concentrations (0.01−1 mM). Using 5-FITP and 5-AITP, we obtained linear rates in product formation at all concentrations tested. Extrapolation of the time course back to time zero does not reveal a burst in primer elongation under pseudo-first-order reaction conditions (Figure 2). Furthermore, burst kinetics were not observed using a higher concentration of gp43 (100 or 200 nM (data not shown)). The lack of an observed "burst" in product formation under pseudo-first-order reaction conditions suggests that phosphoryl transfer or a kinetic step prior to phosphoryl transfer is rate-limiting for enzyme turnover. Regardless, the measured rates of nucleotide incorporation were plotted as a function of dXTP concentration and displayed saturation kinetics (data not shown). Values of k_{pol}, K_D, and k_{pol}/K_D were obtained from the fit of the data to the Michaelis−Menten equation and are summarized in Table 1.

Linear rates in product formation were also observed with 5-PhITP as the nonnatural analogue. However, an apparent burst in primer elongation was observed when 5-PhIMP is inserted opposite the nontemplating lesion (Figure 2). Both the burst in primer elongation and the steady-state rate in product formation were independent of 5-PhITP concentration (data not shown). Collectively, these data are consistent with a mechanism in which a kinetic step *after* phosphoryl transfer is rate-limiting for enzyme turnover.

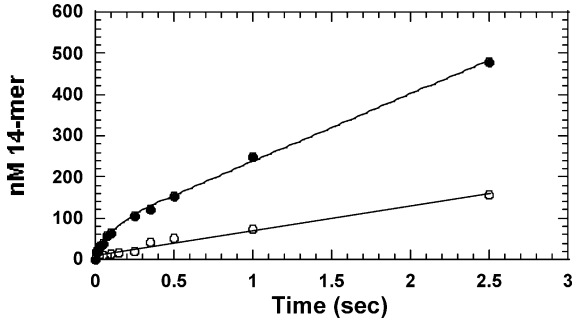

FIGURE 3: Pre-steady-state time courses for the insertion of 5-PhIMP opposite an abasic site (●) or opposite T (○). Assays monitoring translesion DNA synthesis were performed mixing a preincubated solution of 75 nM gp43 exo$^-$ and 2 μM 5′-labeled 13/20SP-mer with an equal volume of a preincubated solution of 10 mM magnesium acetate and 5 μM 5-PhITP in the same reaction buffer (final concentrations). The reaction was then terminated at various times by the addition of 500 mM EDTA at the times demarcated on the graphs. Assays monitoring the insertion of 5-PhIMP opposite T were performed under identical conditions exception that the concentration of 5-PhITP was maintained at 100 μM.

Transient Kinetic Analysis of 5-PhITP Incorporation Opposite an Abasic Site. The results of the manual quenching experiments suggest that the incorporation of 5-PhITP opposite the abasic site is extremely rapid. Therefore, experiments were performed using a rapid-quench instrument (*25*) to unequivocally detect the presence of a "burst" in primer elongation. As illustrated in Figure 3, the time course for 5-PhITP incorporation opposite an abasic site is biphasic as characterized by a rapid initial burst in 14-mer formation followed by a second, slower phase in primer elongation. The second, linear phase of the time course represents release of gp43 from extended DNA and subsequent turnover of remaining 13/20SP-mer. When 5 μM 5-PhITP is used, the observed rate constant of the burst phase is 9.1 ± 2.1 s^{-1} while the k_{cat} value is 2.2 ± 0.5 s^{-1}. The amplitude of the burst phase is equal to the amount of gp43 used in the reaction (75 nM). The detection of a stoichiometric burst even at low concentrations of 5-PhITP suggests that the nonnatural nucleotide binds very tightly to the polymerase/DNA complex such that the gp43/DNA/5-PhITP complex partitions to product (gp43 + DNA_{n+1} + PP_i) rather than collapsing back to gp43/DNA + 5-PhITP (*26*). Alternatively, the stoichiometric burst amplitude can be explained if the phosphoryl transfer step is favorable such that nucleotide binding and incorporation are driven to completion. To evaluate these potential mechanisms, the kinetic dissociation constant, K_D, as well the maximal polymerization rate, k_{pol}, for the insertion of 5-PhIMP were measured.

Measurements of k_{pol} and K_D for 5-PhITP Incorporation Opposite an Abasic Site. Single turnover conditions were then employed to accurately measure the K_D and k_{pol} values for the insertion of 5-PhIMP opposite the abasic site. Since the concentration of polymerase is maintained in excess versus DNA substrate, these experiments alleviate complications arising from any kinetic step after phosphoryl transfer.

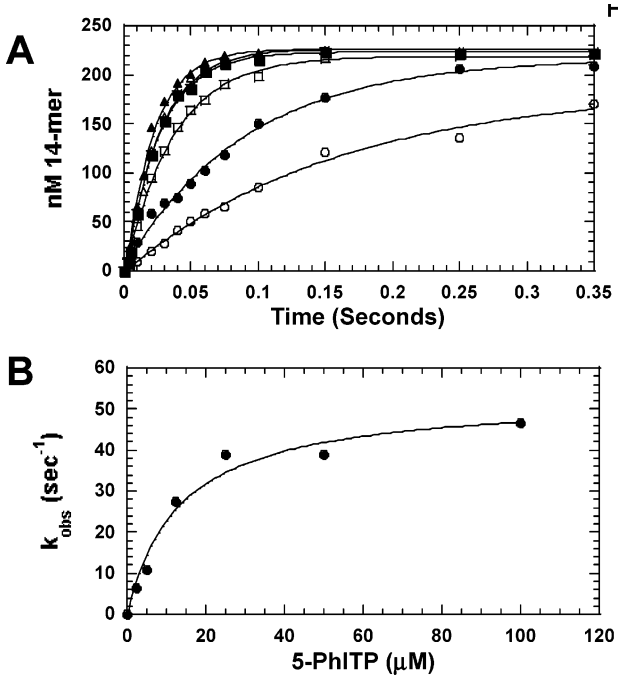

FIGURE 4: Dependency of 5-PhITP concentration on the observed rate constant in primer elongation as measured using single turnover conditions. (A) gp43 exo$^-$ (1 μM) and 5′-labeled 13/20SP-mer (250 nM) were preincubated, mixed with increasing concentrations of Mg^{2+}/5-PhITP to initiate the reaction, and quenched with 500 mM EDTA at variable times (0.005−0.35 s). The incorporation of 5-PhITP was analyzed by denaturing gel electrophoresis. 5-PhITP concentrations were 2.5 (○), 5 (●), 12.5 (□), 25 (■), 50 (△), and 100 μM (▲). The solid lines represent the fit of the data to a single exponential. (B) The observed rate constants for 5-PhIMP insertion (●) were plotted against 5-PhITP concentration and fit to the Michaelis−Menten equation to determine values corresponding to K_D and k_{pol}.

This allows for the measurement of the kinetic steps reflecting initial ground state binding of 5-PhITP, the conformational change prior to phosphoryl transfer, and phosphoryl transfer itself. All time courses were generated using a rapid quench instrument as previously described (*14*).

Representative data for the concentration dependency of 5-PhITP on the rate constant in primer elongation are presented in Figure 4A. All time courses were fit to the equation for a single-exponential process to define k_{obs}, the rate constant in product formation. The plot of k_{obs} versus 5-PhITP concentration is hyperbolic (Figure 4B) from which values of $k_{pol} = 53 \pm 4$ s^{-1} and $K_{D\ 5-PhITP} = 14 \pm 3$ μM were obtained.[2] Values are summarized in Table 1.

The Effects of Acid versus EDTA Quenching on the Kinetics of 5-PhITP Incorporation Opposite an Abasic Site.

Scheme 1: Kinetic Mechanism of gp43 exo−, the Bacteriophage T4 DNA Polymerase[a]

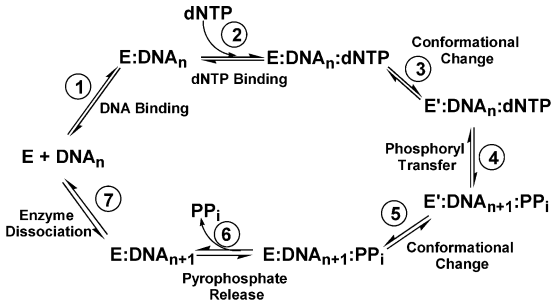

[a] Individual steps along the pathway for DNA polymerization are numbered and identified. Abbreviations are as follows: E = T4 DNA polymerase; DNA_n = DNA substrate; E′ = conformational change in DNA polymerase; PP_i = inorganic pyrophosphate; DNA_{n+1} = DNA product (DNA extended by one nucleobase).

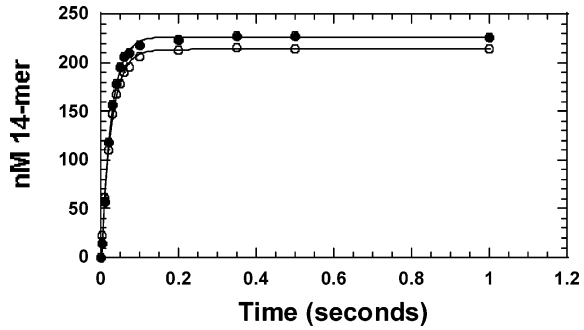

FIGURE 5: Rapid quench kinetic time courses for the incorporation of 5-PhITP opposite an abasic site using EDTA (●) or HCl (○) as the quenching reagent. The gp43 exo$^-$ (1 μM) and 5′-labeled 13/20SP-mer (250 nM) were preincubated, mixed with 10 mM Mg^{2+} and 30 μM 5-PhITP to initiate the reaction, and quenched with either 500 mM EDTA or 1 M HCl at variable times (0.005−0.35 s). After quenching with HCl, 100 mL of phenol/chloroform/iso-amyl alcohol was added to extract the polymerase, and the pH of the aqueous phase was neutralized with the addition of 1 M Tris/3 M NaOH. Product formation was analyzed by denaturing gel electrophoresis followed by phosphorimaging analysis. A burst amplitude of 240 ± 6 nM and a k_{obs} of 38.4 ± 2.1 s^{-1} were obtained using EDTA as the quench, while a burst amplitude of 220 ± 3 nM and a k_{obs} of 37.4 ± 1.4 s^{-1} were obtained using HCl as the quench.

We argue that the increase in the k_{pol} value represents an enhancement in the conformational change step prior to phosphoryl transfer. However, it is also possible that the phosphoryl transfer step is rate-limiting for the incorporation of the nonnatural nucleotide opposite the abasic site. To evaluate this possibility further, time courses in 5-PhITP incorporation were generated under single turnover conditions using either a nondenaturing quench (EDTA) or a denaturing agent (hydrochloric acid). Differences in the amount of product formation can be observed using these quenching agents since EDTA stops the reaction only after a full catalytic cycle while hydrochloric acid kills all enzyme forms that accumulate along the reaction pathway. According to Scheme 1, these enzyme forms include E:DNA, E:DNA:dXTP, and E′:DNA:dXTP that can accumulate before the chemical step. Therefore, a reduced burst amplitude in product formation should be observed using the denaturing quench if the phosphoryl transfer step is rate-limiting for incorporation. As shown in Figure 5, time courses generated for the incorporation of 30 μM 5-PhITP opposite the abasic site are nearly identical with either quenching agent. In both

[2] It was reported earlier that when 5 μM 5-PhITP was used, a burst rate (k_{obs}) of 9 s^{-1} was measured for incorporation opposite the abasic site under pseudo-first-order reaction conditions. This value is significantly less than the reported k_{pol} value of 53 s^{-1} measured using single turnover reaction conditions. The lower value of 9 s^{-1} reflects the fact that the concentration of 5 μM 5-PhITP is below the K_D value of 5-PhITP. To validate this conclusion as well as to demonstrate consistency between experiments performed using pseudo-first-order versus single turnover conditions, we applied these rate and dissociation constants to the Michealis−Menten equation ($k_{obs} = k_{pol}$[5-PhITP]/(K_D + [5-PHITP])). Using a k_{pol} value of 53 s^{-1} and a K_D of 14 μM, we calculate that the k_{obs} value using 5 μM 5-PhITP is 14 s^{-1} and is in good accord with the measured value of 9 s^{-1} measured independently under pseudo-first-order reaction conditions.

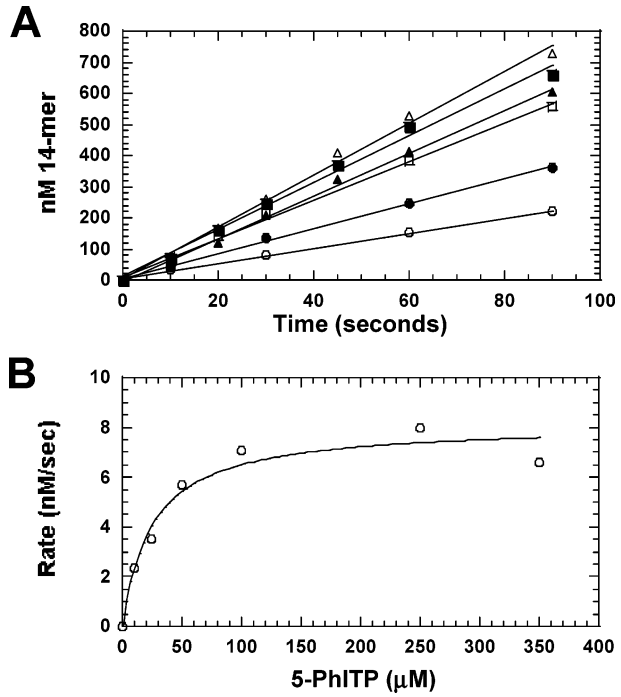

FIGURE 6: Dependency of 5-PhITP concentration on incorporation opposite T as measured under pseudo-first-order reaction conditions. (A) gp43 (50 nM) and 5′-labeled 13/20SP-mer (1 μM) were preincubated, mixed with increasing concentrations of Mg^{2+}/5-PhITP to initiate the reaction, and quenched with 200 mM EDTA at variable times (5−120 s). The insertion of 5-PhIMP was analyzed by denaturing gel electrophoresis. 5-PhITP concentrations were 10 (○), 25 (●), 50 (□), 100 (▲), 250 (■), and 350 μM (△). The solid lines represent the fit of the data to a straight line. (B) The observed rates for Ind-MP insertion (O) were plotted against 5-PhITP concentration and fit to the Michaelis−Menten equation to determine values corresponding to K_D and k_{pol}.

cases, the rate constants for incorporation are essentially identical (37.4 ± 1 s^{-1} with EDTA versus 38.4 ± 2.1 s^{-1} with HCl). However, there is an 8.3% difference in burst amplitudes that is dependent upon the nature of the quenching agent. When EDTA is used, the burst amplitude is 240 ± 6 nM while that when HCl is used is 220 ± 3 nM. The potential significance of this slight difference on identification of the rate-limiting step in nucleotide incorporation is discussed later.

Kinetic Parameters for Insertion Opposite Templating Nucleobases. Values for k_{pol}, K_D, and k_{pol}/K_D were also measured for the incorporation of 5-PhITP, 5-FITP, and 5-AITP opposite any natural templating nucleobase. For each nonnatural nucleotide tested, linear rates in product formation are observed at all concentrations tested regardless of templating base composition, that is, insertion opposite A, C, G, or T. Representative data for the insertion of 5-PhIMP opposite T provided in Figure 6 reveals that defined "bursts" in primer elongation are not observed for 5-PhIMP insertion opposite T or any other natural templating nucleobase (data not shown). The lack of a burst phase precludes definition of an accurate k_{obs} value for insertion. Regardless, the lack of a defined burst again suggests that phosphoryl transfer or a kinetic step prior to phosphoryl transfer is rate-limiting for their insertion. Values for k_{pol}, K_D, and k_{pol}/K_D were obtained as described above and are summarized in Table 2.

Table 2: Summary of Kinetic Rate and Equilibrium Constants for the Insertion of 5-Phenyl-indolyl-2′-deoxyriboside Triphosphate, 5-Fluoro-indolyl-2′-deoxyriboside Triphosphate, and 5-Amino-indolyl-2′-deoxyriboside Triphosphate Opposite Templating Bases[a]

dXTP	template	k_{pol} (s^{-1})	K_D (μM)	k_{pol}/K_D (M^{-1} s^{-1})
5-PhITP	A	0.12 ± 0.01	30 ± 10	4.0×10^3
5-PhITP	C	0.19 ± 0.02	28 ± 7	6.8×10^3
5-PhITP	G	0.26 ± 0.02	12 ± 4	21.7×10^3
5-PhITP	T	0.16 ± 0.01	25 ± 7	6.4×10^3
5-FITP	A	0.11 ± 0.06	170 ± 28	0.6×10^3
5-FITP	C	*b*	*b*	*b*
5-FITP	G	*b*	*b*	*b*
5-FITP	T	0.040 ± 0.003	141 ± 32	0.29×10^3
5-AITP	A	0.21 ± 0.01	263 ± 102	0.46×10^3
5-AITP	C	*b*	*b*	*b*
5-AITP	G	*b*	*b*	*b*
5-AITP	T	0.071 ± 0.003	132 ± 21	0.53×10^3

[a] The kinetic parameters, k_{pol}, K_D, and k_{pol}/K_D, for each nonnatural nucleotide were obtained under pseudo-first-order reaction conditions using 50 nM gp43exo$^-$, 1 μM 13/20SP-mer, and 10 mM Mg^{2+} at varying concentrations of nonnatural nucleotide triphosphate (0.01−1 mM). [b] Not determined since incorporation was not observed at 1 mM nucleotide, the highest concentration tested.

DISCUSSION

Several models have been proposed to account for the preferential insertion of purines opposite an abasic site (*14*, *27*−*29*). Among these include the involvement of hydrophobic effects and entropic compensation (*27*) as well as steric constraints and shape complementarity (*28*). However, an alternative model is the involvement of base-stacking contributions of the incoming nucleobase (*14*, *29*). We previously provided evidence for this model by demonstrating that the incorporation of 5-NITP, a novel nucleobase possessing enhanced base-stacking abilities (*14*), is 1000-fold more efficient compared to that for natural nucleobases such as dAMP and dGMP (*13*). Furthermore, replacement of the nitro moiety with −H reduces the rate of insertion by 3 orders of magnitude (*16*) and suggests that the π-electron density of the nitro group plays a major role toward enhancing incorporation opposite an abasic site. In this report, we have further evaluated the contributions of π-electron stabilization through a structure−activity relationship study using various 5-substituted indole triphosphates.

π-Electron Contributions during Catalysis. Our analysis begins by revisiting the established kinetic mechanism of gp43 exo$^-$ (Scheme 1) (*17*). In this multistep reaction pathway, there are two microscopic steps that are the most significant contributors toward catalysis and fidelity. These include the binding of dNTP to the polymerase/nucleic acid complex and the subsequent conformational change preceding phosphoryl transfer. Proper dNTP binding has historically been attributed to the formation of Watson−Crick base pairs between the incoming dNTP and template nucleobase (Scheme 1, step 2) (reviewed in refs *30* and *31*). The formation of correctly paired partners is energetically favorable and typically exemplified by $K_{D\ dNTP}$ values in the low micromolar range. Upon binding the correct dNTP, the polymerase/DNA complex then undergoes a conformational change (Scheme 1, step 3) to further align the incoming dNTP into the correct geometrical arrangement for subsequent phosphoryl transfer (Scheme 1, step 4). During correct

DNA synthesis, the rate constant for this conformational change has been experimentally measured at ~100 s^{-1} and is at least 10-fold slower than the rate constant for phosphoryl transfer (*17*, *18*). Thus, the conformational change step is rate-limiting for the first round of enzyme turnover during normal DNA replication.

During translesion synthesis, however, both ground-state binding of dNTP and the subsequent conformational change are highly disfavored (*13*). Although the K_D for natural dNTPs is elevated severalfold, the predominant parameter that kinetically hinders misinsertion is the large reduction in the k_{pol} values. For example, k_{pol} values of ~0.02−0.1 s^{-1} have been reported for the misincorporation of natural dNTPs opposite the abasic site (*13*) and represent a 10^3−10^4-fold reduction compared to those values measured for the formation of natural Watson−Crick base pairs (*17*, *18*). The reduction in rate constant could reflect the lack of hydrogen-bonding interactions or shape complementarity associated with the lack of coding information present at an abasic site. However, the fast k_{pol} value of ~50 s^{-1} measured here for the incorporation of 5-PhITP and that of ~120 s^{-1} reported for the incorporation of 5-NITP (*14*) opposite an abasic site suggest that the rate constant for polymerization can be accelerated if the incoming nucleobase contains an extended π-electron surface area. We argue that the increase in the k_{pol} value represents an enhancement in the conformational change step prior to phosphoryl transfer. However, there is still debate as to whether the phosphoryl transfer step is at least partially rate-limiting for the incorporation of the nonnatural nucleotides opposite the abasic site. This issue was evaluated by measuring the time courses in 5-PhITP incorporation using EDTA (a nondenaturing quench) versus HCl (a denaturing agent). As outlined before, a lower burst amplitude should be obtained using HCl if phosphoryl transfer is rate-limiting since any enzyme forms that accumulate before the chemistry step will be effectively quenched by this denaturant while EDTA will quench the reaction only after the first turnover of the polymerase. The time courses presented in Figure 5 are nearly identical. In both cases, the rate constants in incorporation are identical at ~38 s^{-1}. In contrast, the maximal amount of product formed using EDTA is slightly higher (~8%) than that using HCl as the quenching agent. We argue that this difference is minimal and suggests that phosphoryl transfer is not rate-limiting for the incorporation of 5-PhITP opposite an abasic site. An argument can, however, be made that this difference may be significant. If correct, then the difference of 8% can be used to calculate the internal equilibrium constant of ~9 for the chemical step. The importance of this value is that it still suggests that phosphoryl transfer may be, at most, partially rate-limiting for the incorporation of 5-PhITP opposite the abasic site. We note that further experiments such as pulse−chase will be required to completely validate that phosphoryl transfer does not completely limit nucleotide incorporation.

These data provide evidence that the conformational change step may be completely rate-limiting for 5-PhITP incorporation opposite an abasic site. We argue that this conformational change step reflects the enzymatic motions required to reposition the incoming nucleobase from an extrahelical position into an interhelical position. This mechanism is intuitive at the molecular level if one considers

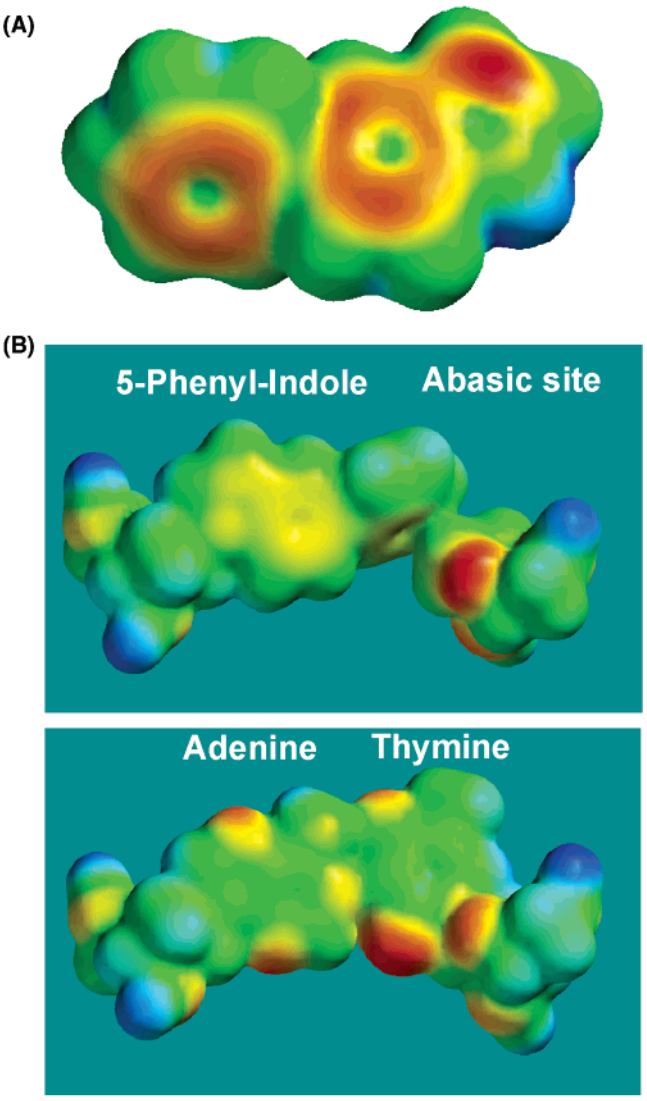

FIGURE 7: (A) Computer-generated model for 5-phenyl-indole-deoxyribose. Electrostatic surface potentials were generated using Spartan '04 software. Red indicates the highest electronegative regions, green is neutral, and blue indicates electropositive regions. The partial atomic charges were calculated using Hartree−Fock 3-21G(*) (displayed) or the AM1 model (data not shown). (B) Computer-generated model comparing the structures of base pairs corresponding to 5-phenyl-indole-deoxyribose monophosphate paired opposite an abasic site (top) with that for adenine deoxyribose monophosphate paired opposite thymine deoxyribose monophosphate (bottom). Electrostatic surface potentials were generated using Spartan '04 software as described above.

that an incoming nucleobase containing extensive π-electrons would be thermodynamically favored to exist in the interior of duplex DNA due to offset base-stacking contributions. Indeed, computer models for the structure of the 5-phenyl-indole deoxyriboside provided in Figure 7A show that the molecule has an extended π-electron cloud that is not localized to any significant extent. It is noteworthy that the most energetically favorable conformation is that in which the phenyl substituent is tilted 26.8° out-of-plane with respect to the indole moiety. Molecular modeling of the nonnatural nucleoside placed opposite the abasic site reveals that this subtle distortion has a minimal effect on the overall shape of the pair in comparison to a natural A:T base pair (Figure 7B). Thus, the overall shape and stacking contributions of 5-phenyl-indole opposite an abasic site are predicted to be

in an optimal arrangement for stable incorporation. Although the shape and size of 5-phenyl-indole opposite an abasic site appear important for the rate enhancement for incorporation, we argue that it is not the predominant driving force. Specifically, both 5-PhITP and 5-NITP are rapidly incorporated opposite an abasic site despite having significant differences in shape and size (compare 223.2 Å^2 for 5-PhITP versus 171.4 Å^2 for 5-NITP). If shape complementarity were the sole driving force, then 5-PhITP should be incorporated more efficiently than 5-NITP since it more adequately fills the void of an abasic site. We argue that π-electron surface area, the most notable common feature between the two analogues, plays the most significant role for their facile incorporation opposite an abasic site.

Further evidence of the importance of π-electron surface area comes from evaluation of the insertion of other 5-substituted indoles such as 5-FITP and 5-AITP opposite an abasic site. Although fluorine possesses electron-withdrawing potential similar to that of a nitro group, it does not possess significant π-electron density. In fact, this deficiency can explain the poor kinetics for 5-FIMP insertion opposite the abasic site. A similar line of reasoning can be applied to the amino derivative, 5-AITP. In this case, the amino group is similar in size to a nitro group and also possesses a hydrogen-bond donor group. However, 5-AITP lacks an extended π-electron surface area and is inserted poorly opposite an abasic site. As summarized in Table 1, the catalytic efficiency for 5-FITP and 5-AITP insertion opposite the abasic site is low. Both nonnatural nucleotides display low k_{pol} values of $\sim$0.3 s^{-1} that are remarkably similar to those values reported for the incorporation of dATP (*13*) and IndTP (*16*), respectively. These results collectively suggest that π-electron contributions rather than electronegativity, size constraints, or hydrogen-bonding interactions gives rise to enhanced selectivity for insertion opposite the nontemplating lesion (refer to Supporting Information for computer models for 5-fluoro- and 5-amino-indole deoxyribosides).

π-Electron Interactions Are Required for Optimal Ground-State Binding. We envision that the conformational change step outlined in Scheme 1 reflects the ability of the polymerase to "stack" the nucleobases into the interior of the DNA helix. However, the question still remains as to whether (and how) the presence of π-electrons affects ground-state binding of the incoming nucleotide. It was previously demonstrated that the low K_D value of $\sim$20 μM for 5-NITP was independent of templating nucleobase (*14*). This result was interpreted to reflect the existence of a "nonselective" dNTP-binding site in gp43 composed of highly conserved aromatic amino acids that could stabilize the binding of the incoming nucleobase through $\pi-\pi$ stacking interactions (*31*, *33*−*35*). The kinetic data presented in this manuscript provide additional support for this mechanism. Specifically, the K_D value for 5-PhITP incorporation opposite an abasic site is 14 μM and is essentially identical to that measured for 5-NITP (*14*). The identity in binding affinities coincides strongly with the high degree of electron conjugation associated with each molecule. As illustrated in Figure 8, the active site of the DNA polymerase from bacteriophage RB69[3] is lined with several aromatic amino acids that are within 10 Å of the primer−template junction (*31*, *33*, *34*). The extended π-electron density of 5-phenyl-indole could interact favorably with the aromatic amino acids lining the active site of the DNA polymerase. We propose that these previously unrecognized interactions may play an important role in catalysis during translesion DNA synthesis. Indeed, mutagenesis of Y416 to serine dramatically reduces the catalytic efficiency for the incorporation of 5-NITP and 5-PhITP opposite the abasic site lesion while it has little effect on the correct incorporation of dATP opposite T (unpublished data, A.J.B. and B. Devadoss). The reduced efficiency during translesion DNA synthesis is consistent with the loss of base-stacking interactions in the enzyme's active site.

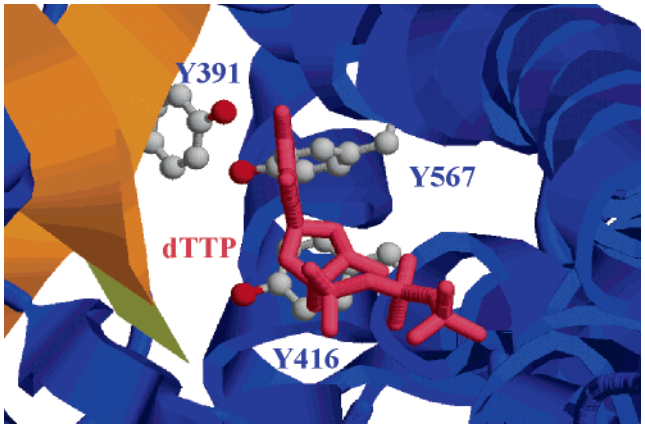

FIGURE 8: Model for proposed $\pi-\pi$ stacking interactions of the incoming dNTP with aromatic amino acids in the active site of RB69 DNA polymerase (*30*). For clarity, the conserved aromatic amino acids of the DNA polymerase are colored in blue. The 3′-terminal of DNA duplex is colored yellow. The coming dTTP, colored in pink, is shown as a stick model.

The measured K_D values for 5-FITP and 5-AITP insertion opposite the abasic site provide additional insight into the dynamics of nucleotide binding. Replacement of π-electrons with either an electron-withdrawing group (5-fluoro derivative) or a group capable of providing hydrogen-bonding interactions (5-amino derivative) reduces binding affinity by at least 10-fold (Table 3). This reduction corresponds to a change in relative free energy of $\sim$1.4 kcal/mol that potentially represents the energy associated with $\pi-\pi$ stacking. Removal of π-electron density at the 5-position of indole could easily reduce the strength between the interactions of the incoming nucleobase with these active site residues to adversely affect binding affinity.

Alternative Models for Translesion DNA Synthesis. Alternative mechanisms invoking the involvement of desolvation, dipole moment, or both could also account for the preferential insertion of 5-NIMP and 5-PhIMP opposite the abasic site. If desolvation were the most critical parameter, then the efficiency of insertion should correlate well with the hydrophobicity (log *P*) of the nucleobase. This model predicts that 5-PhIMP should be inserted opposite an abasic site with a higher overall efficiency compared to 5-NIMP due to the large value of 3.3 of the former nucleobase compared to the lower log *P* of $\sim$1.7 of the latter. As summarized in Table 3, the catalytic efficiency for 5-PhIMP

[3] The DNA polymerases from bacteriophage T4 and RB69 possess $\sim$60% sequence identity (*35*). Y391, Y416, and Y567 in gp43 from bacteriophage RB69 are equivalent to F388, Y413, and Y564 in gp43 from bacteriophage T4 (*35*).

Table 3: Comparison of Selective Biophysical Parameters of Various 5-Substituted Indole Derivatives

nucleobase	catalytic efficiency[a]	log *P*[b]	dipole moment[c]	surface area (Å^2)[d]	volume (Å^3)[e]	π-electrons[f]
adenine	1.5×10^3	−1.45	2.38	143.0	121.7	no
indole	1.9×10^3	1.64	2.02	146.2	131.1	no
5-nitro-indole	7.0×10^6	1.67	7.81	171.4	152.4	yes
5-phenyl-indole	3.8×10^6	3.31	2.24	223.2	213.4	yes
5-fluoro-indole	2.0×10^3	1.79	4.22	152.0	135.7	no
5-amino-indole	0.5×10^3	0.83	1.00	159.7	141.3	no

[a] Catalytic efficiency is defined as k_{pol}/K_D (M^{-1} s^{-1}) and represents the apparent second-order rate constant of the enzyme catalyzed reaction. These values are taken from Table 1 and references cited within. [b] The log *P* values, the oil-to-water partition coefficients, were calculated using Spartan '02 software and are used as an indicator of relative hydrophobicity. [c] Dipole moments (D) were calculated using Spartan '02 software and are used as an indicator of relative electronegativity. [d] Surface areas were calculated using Spartan '02 software. [e] Volumes were calculated using Spartan '02 software and are used as an indicator of relative size of the nucleobase. [f] The term π-electrons refers to the presence of a conjugated substituent group at the 5 position of indole.

insertion is 2-fold lower than 5-NIMP despite the fact that the log *P* value of 5-phenyl-indole is significantly higher. Further evaluation of other modified indole triphosphates yields identical interpretations. For example, indole deoxyriboside and the 5-fluoro derivative have nearly identical log *P* values compared to 5-NIMP yet are inserted 1000-fold less efficiently. While desolvation undoubtedly plays a significant role during DNA replication by stabilizing duplex DNA (reviewed in ref *1*), it appears to play a minimal role in directly influencing nucleotide insertion during translesion DNA synthesis. Other relevant biophysical parameters such as dipole moment and surface area (Table 3) appear to play minimal roles on an individual basis since a reasonable correlation between the measured catalytic efficiency with either of these parameters is not observed.

The Role of Shape Complementarity during DNA Polymerization. 5-Substituted indoles such as 5-FITP and 5-AITP were expected to be efficiently inserted opposite the pyrimidines, C and T, since they were predicted to form base pairs that resemble Watson−Crick base pairs due to the favorable contributions of steric fit and potential hydrogen-bonding interactions. The data summarized in Table 3 shows a poor correlation between the efficiency of nucleotide insertion and the shape of the formed base pair. This unexpected result is best highlighted by examination of the unfavorable kinetic parameters associated with the insertion of 5-AITP opposite pyrimidines. Despite having a hydrogen-bond donor that could potentially interact with the C4 keto group of thymine, the insertion of 5-AIMP opposite T was very ineffective as manifested in a low k_{pol} ($\sim$0.07 s^{-1}) coupled with a high K_D value ($\sim$130 μM). Likewise, insertion of 5-AIMP opposite C was not detected. This observation is not unique to 5-AIMP insertion since identical trends are also observed for the insertion of 5-FIMP (Table 2).

The most intriguing results are again observed for the insertion of 5-PhIMP opposite any of the templating bases. Although the catalytic efficiency for 5-PhIMP insertion does vary depending upon the composition of templating nucleobase, the measured k_{pol}/K_D values are in most cases 10-fold greater than those measured for 5-FITP and 5-AITP. Surprisingly, the most influential parameter is binding affinity (low K_D values) rather than an enhancement in the rate of the conformational change (low k_{pol} values). The K_D for 5-PhITP is $\sim$25 μM and remarkably similar to the K_D values measured for the incorporation of 5-NITP (*14*). We again propose that the higher binding affinities for nucleotides containing enhanced π-electron contributions is evidence for a "non-specific" binding site for an incoming dNTP that takes advantage of $\pi-\pi$ stacking interactions between the aromatic rings of the incoming dNTP and amino acids. The low k_{pol} values could reflect the impact of shear bulk present on the phenyl ring that most likely precludes stable pairing opposite a template base. This could reflect the contribution of steric fitting/shape complementarity (*36*) or negative selection (*37*).

Conclusion. This report highlights the significant role of π-electron surface area during DNA polymerization, especially during incorporation opposite an abasic site. Perhaps the most intriguing aspect is how the bacteriophage T4 DNA polymerase utilizes the formation of noncovalent bonds between $\pi-\pi$ stacking systems to facilitate nucleotide binding and the conformational change step preceding phosphoryl transfer. A relevant question is whether the influence of π-electrons is "universal" among different DNA polymerases during translesion DNA synthesis? This question cannot be currently answered without some degree of ambiguity. However, preliminary data using the Klenow fragment of *E. coli* DNA polymerase I reveal that this polymerase inserts 5-PhIMP at least 10-fold more efficiently opposite an abasic site than 5-NIMP (unpublished data, A.J.B.). This result appears to contrast data obtained using the bacteriophage T4 enzyme and leads to the provocative suggestion that DNA polymerases utilize different catalytic strategies during DNA polymerization. In this regard, it will be interesting to evaluate whether the Klenow fragment uses shape complementarity as the predominant force for catalysis as proposed (*28*), whereas gp43 utilizes π-electron interactions.

SUPPORTING INFORMATION AVAILABLE

Computer models of 5-fluoro- and 5-amino-indole deoxyribosides. This material is available free of charge via the Internet at http://pubs.acs.org.

REFERENCES

1. Sponer, J., Leszczynski, J., and Hobza, P. (2002) Electronic properties, hydrogen bonding, stacking, and cation binding of DNA and RNA bases. *Biopolymers 61*, 3−31.
2. Horlacher, J., Hottiger, M., Podust, V. N., Hubscher, U., and Benner, S. A. (1995) Recognition by viral and cellular DNA polymerases of nucleosides bearing bases with nonstandard hydrogen bonding patterns. *Proc. Natl. Acad. Sci. U.S.A. 92*, 6329−6333.
3. Moran, S., Ren, R. X., and Kool, E. T. (1997) A thymidine triphosphate shape analogue lacking Watson−Crick pairing ability is replicated with high sequence selectivity. *Proc. Natl. Acad. Sci. U.S.A. 94*, 10506−10511.

4. McMinn, D. L., Ogawa, A. K., Wu, Y. O., Shultz, P. G., and Romesberg, F. E. (1999) Efforts toward the expansion of the genetic alphabet: DNA polymerase recognition of a highly stable, self-pairing hydrophobic base. *J. Am. Chem. Soc. 121*, 11585−11586.
5. Mitsui, T., Kimoto, M., Harada, Y., Sato, A., Kitamura, A., To, T., Hirao, I., and Yokoyama, S. (2002) Enzymatic incorporation of an unnatural base pair between 4-propynyl-pyrrole-2-carbaldehyde and 9-methyl-imidazo [(4, 5)b]pyridine into nucleic acids. *Nucleic Acids Res.* (Suppl. 2), 219−220.
6. Matray, T. J., and Kool, E. T. (1999) A specific partner for abasic damage in DNA. *Nature 399*, 704−709.
7. Randall, S. K., Eritja, R., Kaplan, B. E., Petruska, J., and Goodman, M. F. (1987) Nucleotide insertion kinetics opposite abasic lesions in DNA. *J. Biol. Chem. 262*, 6864−6870.
8. Avkin, S., Adar, S., Blander, G., and Livneh, Z. (2002) Quantitative measurement of translesion replication in human cells: evidence for bypass of abasic sites by a replicative DNA polymerase. *Proc. Natl. Acad. Sci. U.S.A. 99*, 3764−3769.
9. Shibutani, S., Takeshita, M., and Grollman, A. P. (1997) Translesional synthesis on DNA templates containing a single abasic site. A mechanistic study of the "A rule". *J. Biol. Chem. 272*, 13916−13922.
10. Paz-Elizur, T., Takeshita, M., and Livneh, Z. (1997) Mechanism of bypass synthesis through an abasic site analogue by DNA polymerase I. *Biochemistry 36*, 1766−1773.
11. Takeshita, M., Chang, C. N., Johnson, F., Will, S., and Grollman, A. P. (1987) Oligodeoxynucleotides containing synthetic abasic sites. Model substrates for DNA polymerases and apurinic/apyrimidinic endonucleases. *J. Biol. Chem. 262*, 10171−10179.
12. Cai, H., Bloom, L. B., Eritja, R., and Goodman, M. F. (1993) Kinetics of deoxyribonucleotide insertion and extension at abasic template lesions in different sequence contexts using HIV-1 reverse transcriptase. *J. Biol. Chem. 268*, 23567−23572.
13. Berdis, A. J. (2001) Dynamics of translesion DNA synthesis catalyzed by the bacteriophage T4 exonuclease-deficient DNA polymerase. *Biochemistry 40*, 7180−7191.
14. Reineks, E. Z., and Berdis, A. J. (2004) Evaluating the contribution of base stacking during translesion DNA replication. *Biochemistry 43*, 393−404.
15. Loakes, D., and Brown, D. M. (1994) 5-Nitroindole as an universal base analogue. *Nucleic Acids Res. 22*, 4039−4043.
16. Zhang, X., Lee, I., and Berdis, A. J. (2004) Evaluating the contributions of desolvation and base-stacking during translesion DNA synthesis. *Org. Biomol. Chem. 2*, 1703−1711.
17. Capson, T. L., Peliska, J. A., Kaboord, B. F., Frey, M. W., Lively, C., Dahlberg, M., and Benkovic, S. J. (1992) Kinetic characterization of the polymerase and exonuclease activities of the gene 43 protein of bacteriophage T4. *Biochemistry 31*, 10984−10994.
18. Frey, M. W., Nossal, N. G., Capson, T. L., and Benkovic, S. J. (1993) Construction and characterization of a bacteriophage T4 DNA polymerase deficient in 3′→5′ exonuclease activity. *Proc. Natl. Acad. Sci. U.S.A. 90*, 2579−2583.
19. Rush, J., and Konigsberg, W. H. (1989) Rapid purification of overexpressed T4 DNA polymerase. *Prepr. Biochem. 19*, 329−340.
20. Loakes, D., Brown, D. M., Linde, S., and Hill, F. (1995) 3-Nitropyrrole and 5-nitroindole as universal bases in primers for DNA sequencing and PCR. *Nucleic Acids Res. 23*, 2361−2366.
21. Yang, Y., Martin, A., Nelson, D. L., and Regan, J. (1992) Synthesis of some 5-substituted indoles. *Heterocycles 34*, 1169−1175.
22. Yang, Y., and Martin, A. (1992) Synthesis of 5-arylated indoles via palladium-catalyzed cross-coupling reaction of 5-indoylboronic acid with aryl and heteroaryl halides. *Heterocycles 34*, 1395−1398.
23. Smith, C. L., Simmonds, A. C., Felix, I. R., Hamilton, A. L., Kumar, S., Nampali, S., Loakes, D., and Brown, D. M. (1998) DNA polymerase incorporation of universal base triphosphates. *Nucleosides Nucleotides 17*, 541−554.
24. Mizrahi, V., Benkovic, P. A., and Benkovic, S. J. (1986) Mechanism of DNA polymerase I: exonuclease/polymerase activity switch and DNA sequence dependence of pyrophosphorolysis and misincorporation reactions. *Proc. Natl. Acad. Sci. U.S.A. 83*, 5769−5773.
25. Johnson, K. A. (1995) Rapid quench kinetic analysis of polymerases, adenosinetriphosphatases, and enzyme intermediates. *Methods Enzymol. 249*, 38−61.
26. Gilbert, S. P., and Mackey, A. T. (2000) Kinetics: a tool to study molecular motors. *Methods 22*, 337−354.
27. Goodman, M. F., Creighton, S., Bloom, L. B., and Petruska, J. (1993) Biochemical basis of DNA replication fidelity. *Crit. Rev. Biochem. Mol. Biol. 28*, 83−126.
28. Kool, E. T. (2001) Hydrogen bonding, base stacking, and steric effects in DNA replication. *Annu. Rev. Biophys. Biomol. Struct. 30*, 1−22.
29. Taylor, J. S. (2002) New structural and mechanistic insight into the A-rule and the instructional and noninstructional behavior of DNA photoproducts and other lesions. *Mutat. Res. 510*, 55−70.
30. Young, M. C., Reddy, M. K., and Von Hippel, P. H. (1992) Structure and function of the bacteriophage T4 DNA polymerase holoenzyme. *Biochemistry 31*, 8675−8690.
31. Wang, J., Sattar, A. K., Wang, C. C., Karam, J. D., Konigsberg, W. H., and Steitz, T. A. (1997) Crystal structure of a pol alpha family replication DNA polymerase from bacteriophage RB69. *Cell 89*, 1087−1099.
32. Goodman, M. F., Creighton, S., Bloom, L. B., and Petruska, J. (1993) Biochemical basis of DNA replication fidelity. *Crit. Rev. Biochem. Mol. Biol. 28*, 83−126.
33. Franklin, M. C., Wang, J., and Steitz, T. A. (2001) Structure of the replicating complex of a pol alpha family DNA polymerase. *Cell 105*, 657−667.
34. Hogg, M., Wallace, S. S., and Doublie, S. (2004) Crystallographic snapshots of a replicative DNA polymerase encountering an abasic site. *EMBO J. 23*, 1483−1493.
35. Hendsch, Z. S., Jonsson, T., Sauer, R. T, and Tidor, B. (1996) Protein stabilization by removal of unsatisfied polar groups: computational approaches and experimental tests. *Biochemistry 35*, 7621−7625.
36. Kool, E. T. (2002) Active site tightness and substrate fit in DNA replication. *Annu. Rev. Biochem. 71*, 191−219.
37. Chiaramonte, M., Moore, C. L., Kincaid, K., and Kuchta, R. D. (2003) Facile polymerization of dNTPs bearing unnatural base analogues by DNA polymerase alpha and Klenow fragment (DNA polymerase I). *Biochemistry 42*, 10472−10481.

BI050585F